CrossMark

Experimental and modeling investigation of thorium biosorption by orange peel in a continuous fixed-bed column

Ali Gh. Khamseh[1] · Sohrab Ali Ghorbanian[2]

Abstract
In this research work process parameters and breakthrough modeling of thorium biosorption on orange peel in a fixed-bed column has been studied. Some experiments have been done with sorbent diameter, flow rate, bed height and feed inlet concentration. Breakthrough point decreased with decreasing the bed height, increasing feed inlet concentration and increasing flow rate. Meanwhile, sorption capacity increased with decreasing bed height and flow rate. The highest sorption capacity, 87.7 mg/g, occurred in a 0.4–0.8 mm sorbent diameter. The experimental results were fitted by models of Thomas, Yoon–Nelson and Modified Dose–Response (MDR). The MDR model showed better results.

Keywords Biosorption · Thorium · Orange peel · Breakthrough curves · Fixed-bed column · Adsorption mechanism

Introduction

Heavy metal pollution is one of the most important environmental issues in today's world. The growth of industrial activities has exacerbated environmental pollution, and the accumulation of some contaminants such as heavy metals, synthetic compounds, nuclear wastes, etc. has led to the destruction of some ecosystems. Wastewater from mining, extraction and processing of metals is the most important source of heavy metal contamination. Thorium is one of the waste products produced in the nuclear industry due to thorium processing in nuclear fuel that causes environmental pollution [1, 2]. Thorium nitrate after entering the body, mainly in the liver, spleen, and bone marrow, precipitates in the form of hydroxide [3]. Accordingly, removal and retrieval of the thorium in an affordable way is necessary.

Different methods such as ion exchange and solvent extraction are used to remove heavy metals [4, 5]. But the method that is often used to remove heavy metals from water is adsorption [6]. Different adsorbent materials have been used to adsorb thorium, which can include activated carbon, zeolites [7], gibbsite [8], alumina and silica [9], and molecular sieve powders [10]. Due to the high cost of these adsorbents, researchers tended to use bio-masses, and especially agricultural waste as bio-sorbents. Biological absorbers have many advantages, such as low cost, high efficiency, low biological and chemical sludge, absorbent and metal recovery capabilities [11–13].

In this study, orange peel, which is a cheap and available material, has been used to absorb thorium in a fixed bed column. Orange peel compositions include pectin, cellulose, and hemicellulose. These components contain various functional groups such as carboxyl, hydroxyl, and the like, which play an important role in the adsorption of heavy metals [14]. In recent decades, studies have been done on the adsorption of other heavy metals using orange peel [15–18].

The purpose of this paper is to evaluate the ability and adsorption capacity of orange peel in the column bisorption of thorium and the effect of process variables such as the size of the adsorbent particles, the flow rate, the concentration of the thorium solution and the adsorbent height in the fixed bed column on the thorium adsorption.

✉ Ali Gh. Khamseh
akhamseh@aeoi.org.ir

[1] Nuclear Fuel Cycle Research School, Nuclear Science and Technology Research Institute, AEOI, P.O. Box 11365-8486, Tehran, Iran

[2] Department of Chemical Engineering, Faculty of Engineering, Tehran University, P.O. Box 11365-4563, Tehran, Iran

Theory

The design of the absorption columnar processes is a prediction of the concentration–time profile, or the deflection curve, for the flow out of the column. The breakthrough time indicates the duration of the absorption progression until the concentration of the column output reaches 0.05 of the inlet concentrations. The ineffective bed time (saturation time) is the time when the outlet concentration of column reaches 0.95 of the inlet concentration and the column operation ends. To obtain the absorption capacity of thorium in the column we can use the following equation [19]:

$$q_{\exp} = \frac{C_0}{M} \int_0^{V_E} \left(1 - \frac{C}{C_0}\right) dV \tag{1}$$

where M is the absorbent weight (g), V is the volume of the solution passing through the column (L), V_E is the total volume of the solution passing through the column that saturates the adsorbent, C is the outlet concentration of the solution from the column (mg/L), and C_0 is the inlet concentration of the solution to the column (mg/L).

The total amount of thorium passing through the column is obtained from the following equation [19]:

$$W_{\text{total}} = \frac{C_0 Q t_{\text{total}}}{1000} \tag{2}$$

The total absorption percentage of thorium is derived from the division of $\int_0^{V_E} \left(1 - \frac{C}{C_0}\right) dV$ to the total passed amount of thorium from the column. In other words, the percentage of adsorbed metal is equal to the ratio of the amount of absorbed metal absorbed to the total passed metal through the column. The percentage of total thorium adsorption is given by (3) [19]:

$$R = \frac{M q_{\text{Exp.}}}{W_{\text{total}}} \times 100 \tag{3}$$

Modeling

To analyze the breakthrough curve in the absorption and matching of laboratory data obtained from experiments conducted in this research, with the help of MATLAB software by Thomas, Yoon–Nelson and Modified Dose–Response (MDR) models, nonlinear fitting was performed and the parameters of each model were calculated.

Using experimental data, the Thomas model can predict the breakthrough curve, i.e., concentration profile versus time (theoretical breakthrough curve), and based on this, determine the amount of adsorbed metal per unit mass of adsorbent in the column. The mathematical expression of the Thomas model is as follows [20]:

$$\frac{C}{C_0} = \frac{1}{1 + \exp\left(\frac{M q_0 k_{\text{Th}}}{Q} - \frac{C_0 k_{\text{Th}}}{1000}\right)} \tag{4}$$

where C_0 and C are the concentrations of metal ion in the inlet and outlet (mg/L) of the column, respectively. k_{Th} is the constant of Thomas model [1/(g min)], Q is the flow rate (mL/min), q_0 is the maximum absorption capacity (mg/g), M is the adsorbent mass (g), and t is the time (min).

The Yoon–Nelson model, which evaluates the performance of the absorption column, is simpler than other models and does not require any information about the system's properties such as absorption type and physical properties of the adsorption bed. The assumption of this model is that the rate of decrease in the probability of absorption of each molecule is proportional to the absorption probability and proportional to the absorption breaking point of the adsorbent. The equation of this model is according to (5) [20]:

$$\frac{C}{C_0} = \frac{\exp(k_{\text{YN}} t - \tau k_{\text{YN}})}{1 + \exp(k_{\text{YN}} t - \tau k_{\text{YN}})} \tag{5}$$

where C_0 and C are the concentrations of the metal ion in the inlet and outlet flow (mg/L), t is the test time (min), k_{YN} (min^{-1}) is the Yoon–Nelson model's constant and τ is the time (min) to reach the concentration to 50% of the initial concentration. The model parameters (τ and k_{YN}) are obtained from model matching with experimental data. Also, τ can be obtained directly from laboratory data and compared with the value obtained from the model.

The Modified Dose–Response model minimizes the error caused by using the Thomas model, especially at low and high levels of the graph. The relationship provided for this model is as follows [21]:

$$\frac{C}{C_0} = 1 - \frac{1}{1 + \left(\frac{C_0 V_e}{q_0 M}\right)^{a_{\text{MDR}}}} \tag{6}$$

where C_0 and C are the concentrations in the inlet flow to and output flow from the column (mg/L), V_e is the volume of the solution passing through the column (L), M is the adsorbent mass (g), q_0 is maximum absorption capacity, and a_{MDR} is the constant of this model.

In order to compare the experimental results with the predicted data with the model, the mean percentage error (ε) has been used. ε is obtained from Eq. (7).

$$\varepsilon\% = \frac{\sum_{i=1}^{N} \left| \frac{\left(\frac{c}{c_0}\right)_{\text{exp.}} - \left(\frac{c}{c_0}\right)_{\text{model}}}{\left(\frac{c}{c_0}\right)_{\text{exp.}}} \right|}{N} \times 100 \tag{7}$$

N represents the number of data.

Materials and methods

Materials

Thorium nitrate, Th(NO$_3$)$_4$.5H$_2$O, hydrochloric acid, nitric acid and sodium hydroxide were purchased from Merck company. In this study, northern Iran orange peel (Thomson cultivar) was used as an adsorbent.

Preparation of adsorbent

First, the orange peels were washed three times with distilled water and then shredded into small pieces and dried in an oven at 70 °C for 24 h. Dried peels were crushed using ball mill and Graded with standard sieve sizes of 4–0.8, 0.8–1.25 and 1.25–2 mm in diameter and used for adsorption experiments.

Experiments

Experiments were carried out using a fixed bed column. This column consists of a glass tube of 1.5 cm in diameter and a height of 15 cm (Fig. 1). Continuous experiments were carried out at ambient temperature (25 °C) and optimum pH (3.8) obtained from discontinuous experiments [18]. In order to find an optimal amount of adsorbent particles size, a set of experiments were carried out in 3 steps with absorbent sizes (0.4–0.8 mm), (0.8–1.25 mm in diameter) and (1.25–2 mm). In these experiments the
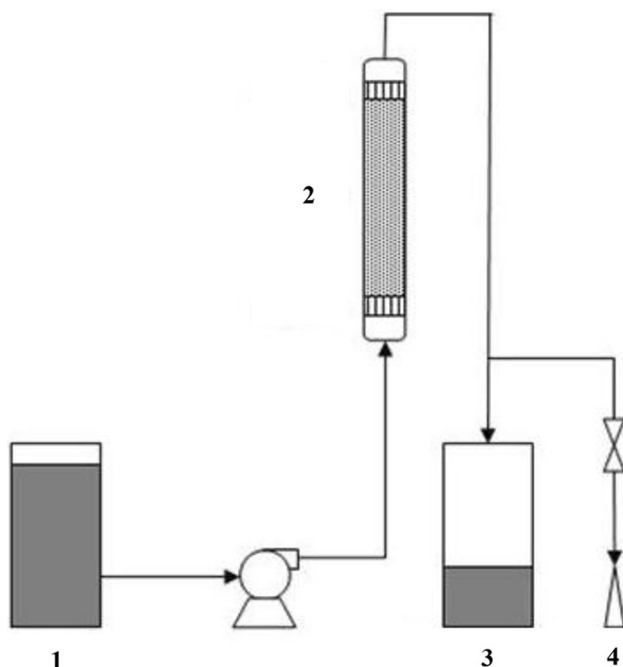
Fig. 1 Laboratory equipment scheme. 1. Tank (input), 2. column, 3. tank (output), 4. sample container

thorium initial thorium solution concentration was 55 mg/L, the flow rate of the solution containing was 1.5 mL/min and the height of the bed was 6 cm.

In order to investigate the effect of the flow rate on the absorption rate, another series of experiments was carried out at a flow rate of 1.5–6 mL/min. To evaluate the effect of the bed height on performance and column adsorption, other sets of experiments were carried out at flow rate of 3 mL/min, concentration of 55 ppm, and three bed heights of 4, 6 and 8 cm. Also thorium solution with initial concentrations of 30, 60 and 90 mg/L was used to investigate the effect of initial concentration of thorium solution on the absorbance under the conditions of the bed height of 6 cm and the flow rate of 3 mL/min.

At the specified time intervals, the column output was sampled and the thorium concentration was determined by inductively coupled plasma spectrometry (PerkinElmer OPTIMA 7300DV ICP optical emission spectrometer). In order to increase the accuracy, all the experiments were repeated two times, and the average of the data was used.

Investigation of the absorption mechanism

FTIR (Oxford, ED2000) analysis was performed to determine the effective groups in thorium adsorption. To investigate the dominant mechanism in biosorption, XRF (Bruker, Veator22) analysis was performed to determine the type and percentage of the elements in the adsorbent before and after the absorption of thorium. To determine the concentration of calcium and potassium ions in the outlet solution over time, experiments were conducted to evaluate the dominant mechanism. Also, the pH of the outlet solution was measured at various initial concentrations, with the start of the absorption process and at specified time intervals.

Results and discussion

The effect of adsorbent particle size

In Fig. 2, the breakthrough curves for the adsorbent with particle sizes of 0.4–0.8, 0.8–1.25, and 1.25–2 mm are presented. According to the results, it was found that the absorbent with particle size 0.4–0.8 mm has the highest absorption (48.74%) and absorption capacity (87.7 mg/g). By decreasing the size of the adsorbent particles, the surface of the adsorbent increases and as a result, the active positions are higher. During the adsorption process, using smaller particle size adsorbents, more metal ions are replaced by adsorbent active sites, which increase the amount of absorption and the time to reach the saturation point. Therefore, according to Fig. 2, it can be said that the
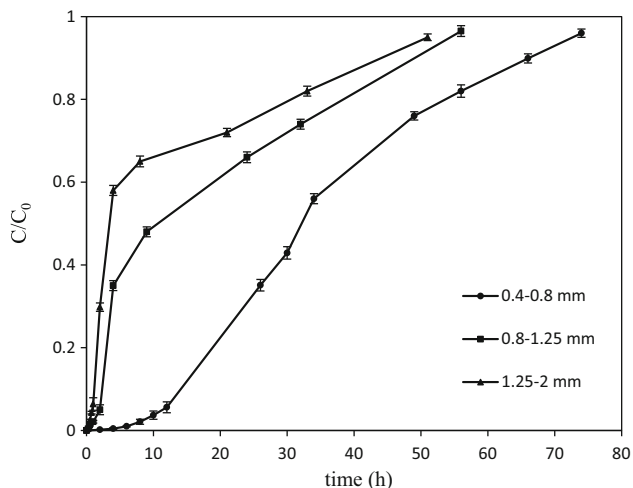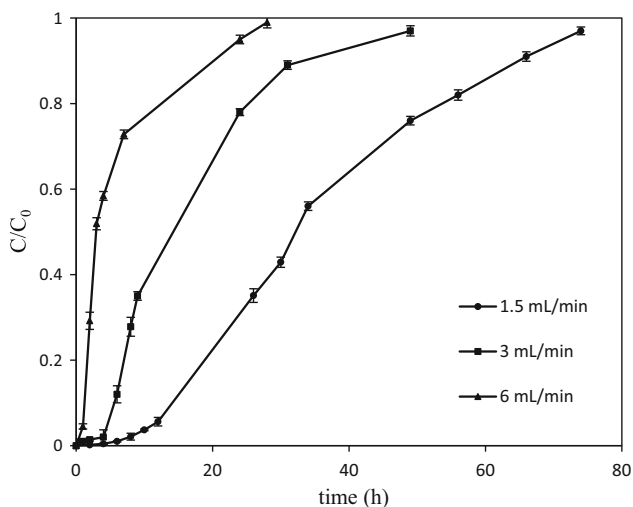
Fig. 2 Breakthrough curves for continuous thorium biosorption at different sizes of adsorbent particles at pH 3.8 and $T = 25$ °C

time of the breakthrough point decreases with increasing the size of the adsorbent particles. If the size of the adsorbent particles is less than the range of 0.4–0.8 mm, due to its low density, low mechanical strength and small particle size, it causes problems such as high pressure drop, swelling and agglomeration of adsorbent. So the adsorbent with a size of 0.4–0.8 mm was selected as a suitable operational size for the bioavailability process.

The effect of flow rate

All three curves obtained from this set of experiments are shown in Fig. 3. As shown in Table 1 and Fig. 3, the breakthrough time, saturation time, and percentage of

Fig. 3 Breakthrough curves for continuous thorium biosorption at different flow rates at pH 3.8 and $T = 25$ °C

thorium adsorption (Table 1) decreased by increasing the flow rate from 1.5 to 6 mL/min. The column absorption capacity is also higher at a flow rate of 1.5 mL/min than the other two flow rates. This is due to lower residence time in the column at flow rates of 3 and 6 mL/min. For this reason, the slope of the flow curves of these two flow rates, i.e. 3 and 6 mL/min, is more intense and reaches the saturation time less than the flow rate of 1.5 ml/min.

The effect of bed height

Each of the three breakthrough curves obtained from this set of experiments is shown in Fig. 4. Absorption capacities at 4, 6 and 8 cm bed heights were 61.03, 73.43 and 71.11 mg/g, respectively (Table 1). As shown in Fig. 4 and Table 1, with increasing the bed height, the breakthrough time and the saturation time increases and the slope of the curves decreases. This is due to the presence of more absorbable sites because of the increased bed height from 4 to 8 cm. Meanwhile at low bed height, i.e. 4 cm, the axial dispersion is dominant in the column and the thorium ions penetration is lower. The thorium solution does not have enough time to penetrate in the adsorbent's pores, and as a result, the adsorption capacity and the absorption percentage are lower.

The effect of inlet concentration

According to Table 1, the amount of absorption capacity for concentrations of 30, 55 and 90 mg/L (flow rate of 3 mL/min and bed height of 6 cm) were 61.7, 73.43 and 79.1 mg/g, respectively. The breakthrough curves obtained from this test are shown in Fig. 5. According to the results, it is shown that in the lower inlet concentrations of thorium solution, the absorption capacity of the column is lower. As it is shown in Fig. 5 and Table 1, breakthrough and saturation times are increased.
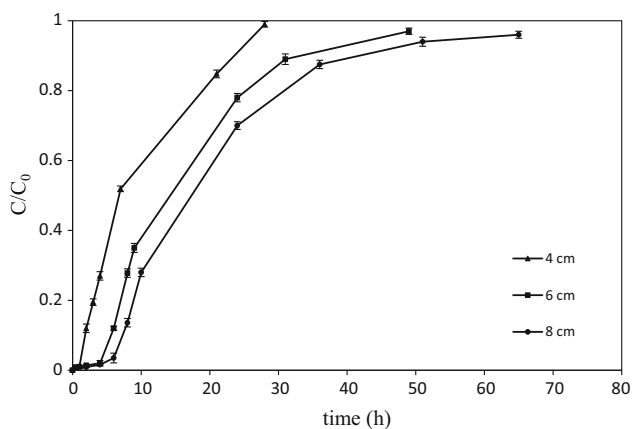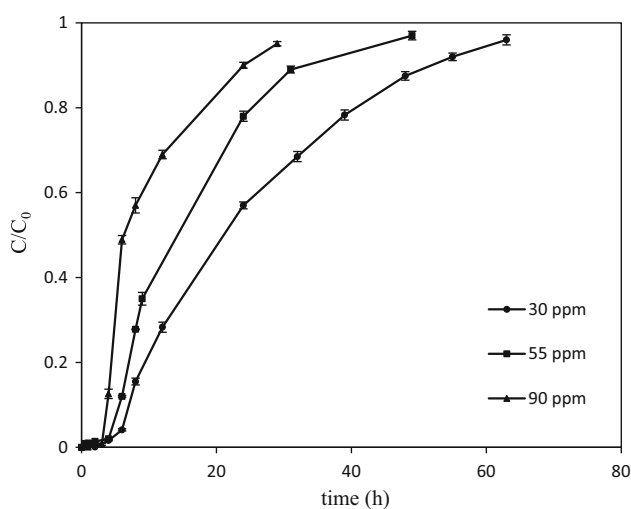
Modeling breakthrough curves

Thomas model

The breakthrough curves obtained from the Thomas model and experimental results for comparison are shown in Fig. 6. Also, the Thomas constant, maximum absorption capacity, absorption capacity obtained from laboratory results, regression coefficient and relative error percentage are presented in Tables 2 and 3. With respect to the results of modeling, using the Thomas model, it turns out that the Thomas constant (k_{Th}) increases with the increase in the size of the adsorbent particles and the flow rate, but decreases with increasing bed height.

Table 1 Operating conditions and experimental results obtained from the thorium breakthrough point s at pH 3.8 and $T = 25$ °C

Flow rate–concentration–height (mL/min–mg/L–cm)	Absorbent size (mm)	Breakthrough point (min)	Saturation point (min)	q_{exp} (mg/g)	Thorium biosorption (%)
1.5–55–6	0.4–0.8	682.1	4440	87.70	48.74
1.5–55–6	0.8–1.25	120	3360	39.56	32.82
1.5–55–6	1.25–2	50	3060	28.00	27.72
3–55–6	0.4–0.8	276	2670	74.43	38.40
6–55–6	0.4–0.8	61.2	1515	58.29	26.58
3–55–4	0.4–0.8	81.5	1562	61.03	32.83
3–55–8	0.4–0.8	377.8	3900	71.11	36.47
3–30–6	0.4–0.8	369.5	3728.9	67.70	38.00
3–90–6	0.4–0.8	201.7	1740	79.10	41.91

Fig. 4 Breakthrough curves for continuous thorium biosorption at different bed heights at pH 3.8 and $T = 25$ °C

Fig. 5 Breakthrough curves for continuous thorium biosorption at different inlet concentrations at pH 3.8 and $T = 25$ °C

Yoon–Nelson model

The obtained parameters and also the results of this model with the experimental results are presented in Fig. 7, Tables 2 and 3. From the results, the k_{YN} value decreases with increasing the bed height, and τ value increases. By increasing the size of the adsorbent particles and flow rate of the solution, the k_{YN} and τ values increase and decrease respectively.

Modified response rate model (MDR)

The results are presented in Fig. 8, Tables 2 and 3. According to Table 2 and Fig. 8, this model gives very good results in all operating conditions. According to the results, "a_{MDR}" decreases with the increase in the adsorbent diameter and the flow rate, and increases with increasing the inlet concentration and the bed height. q_0 values are less than experimental values in all cases.

Thorium biosorption mechanism

The orange peel FTIR spectrum is shown in Fig. 9. In all FTIR spectra, the peak of the hydroxyl group (–OH) ranges from 3424 to 3450 cm^{-1}, the C=O bond of non-ionic carboxylic acids in the range 1735–1750 cm^{-1}, the symmetric and asymmetric bonding of C=O vibration of ionic carboxylate group in the range of 1617–1637 cm^{-1}, and the symmetrical vibration of ionic carboxylic group in the range of 1300–1500 cm^{-1} [22].

The peak shown in the 3440 cm^{-1} shows the presence of free hydrogen or the O–H bond in alcohols, phenols and carboxylic acids present in pectin, cellulose and lignin. As shown in Fig. 9, this peak has changed 8 units in the orange peel after absorption, which indicates effect of this group on the absorption of thorium. The 1741 cm^{-1} peak is
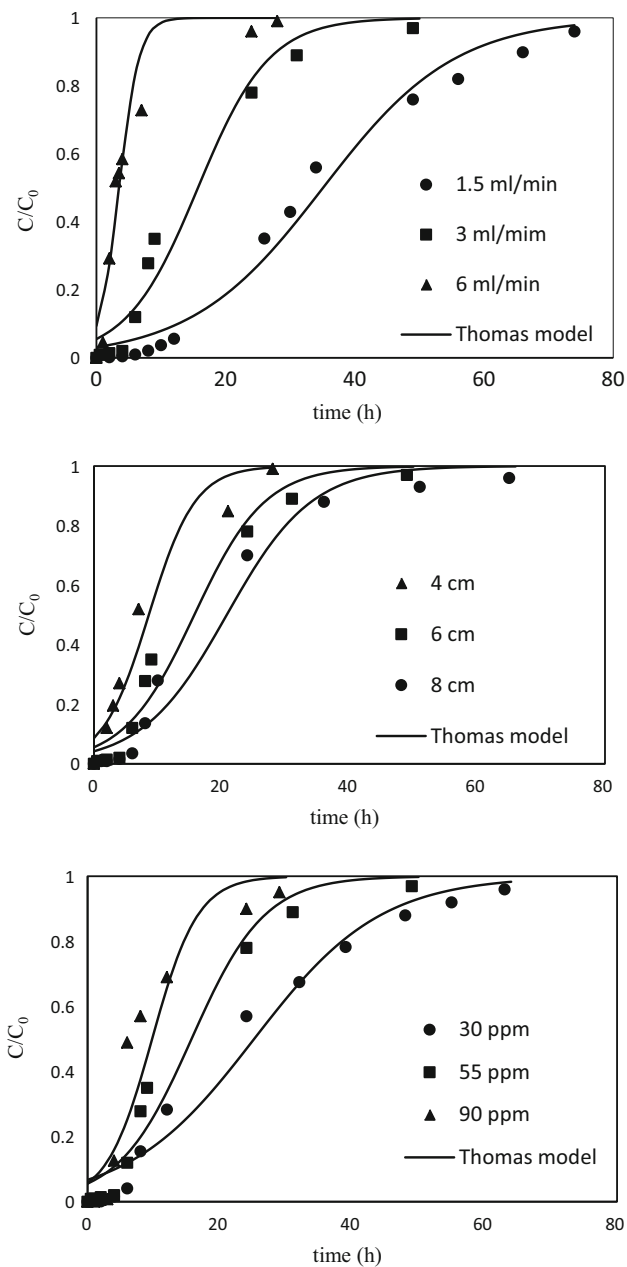
Fig. 6 Breakthrough curves for continuous thorium biosorption under different operating conditions with Thomas model at pH 3.8 and $T = 25\ °C$

Table 2 Operating conditions, constants and errors of models Thomas, Yoon–Nelson and MDR (pH 3.8, $T = 25\ °C$ and absorbent particle size of 0.4–0.8 mm)

| Flow rate	Height	Conc.	Thomas				Yoon–Nelson				MDR			
			q_0	k_{Th}	R^2	$\varepsilon\%$	τ	k_{YN}	R^2	$\varepsilon\%$	q_0	a	R^2	$\varepsilon\%$
1.5	6	55	85.02	0.02981	0.9826	46.1	2061	0.00164	0.9826	43.66	82.3	3.034	0.996	25.19
3	6	55	68.22	0.05479	0.9684	66.42	614.8	0.00783	0.9580	30.0	54.91	2.294	0.9958	41.4
6	6	55	30.44	0.1955	0.9300	41.7	21.03	0.01075	0.9300	41.98	31.56	1.582	0.9822	20.77
3	4	55	55.19	0.08344	0.9493	57.3	400.5	0.00737	0.9683	66.0	45.5	1.775	0.9927	31.42
3	8	55	66.37	0.04564	0.9698	47.2	1168	0.00269	0.9720	31.8	53.65	2.298	0.9954	34.88
3	6	30	59.60	0.05812	0.9645	70.4	1510	0.00174	0.9645	103	50.2	2.013	0.9948	21

related to the vibration of the C=O bond in the non-ionic carboxyl groups (–COOH and –COOCH$_3$) or to the ester or carboxylic group [22]. C-O bond is observed at 1062–1070 cm^{-1} peaks, which are due to the C–OH bond of alcohol and carboxylic groups [23]. Due to the FTIR spectrum of orange peel, the effect of hydroxyl and carboxylic groupings, that are abundantly present in this adsorbent, is known in the biosorption of thorium. The absorption of thorium on orange peel is most likely due to

Table 3 The constants and errors of the models Thomas, Yoon–Nelson and MDR based on the particle size (pH 3.8, $T = 25$ °C, flow rate of 1.5 mL/min, in, initial concentration of 55 mg/L and bed height of 6 cm)

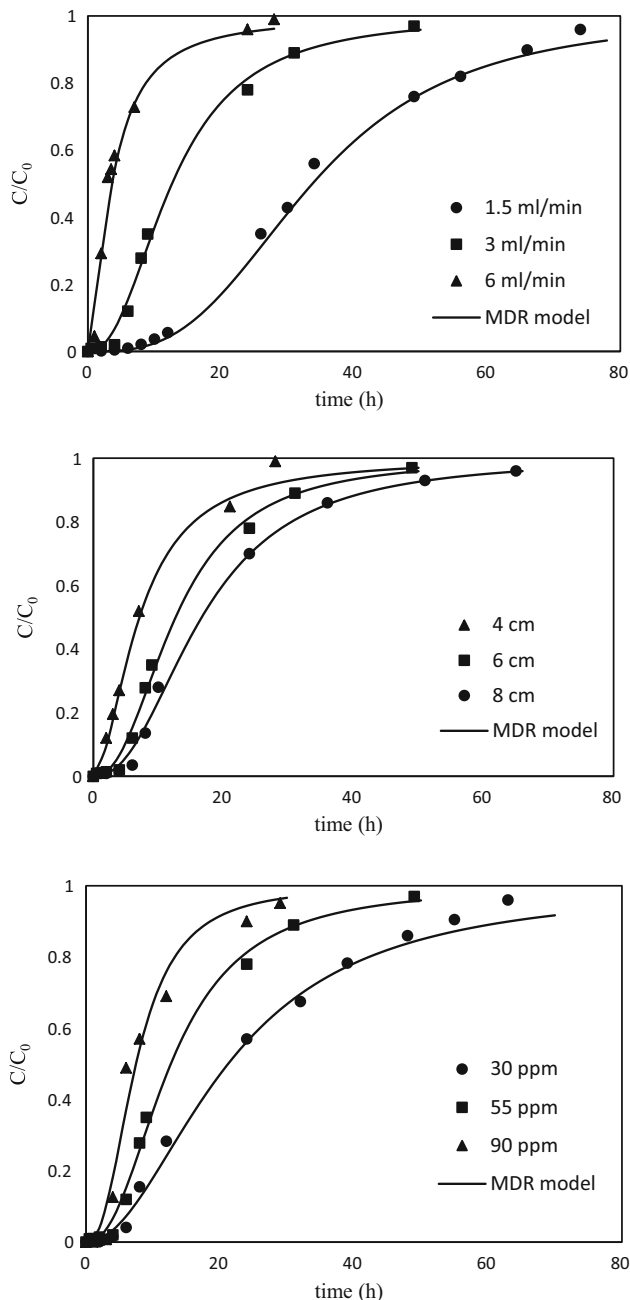| Absorbent particle size (mm)	Thomas				Yoon–Nelson				MDR			
	q_0	k_{Th}	R^2	$\varepsilon\%$	τ	k_{YN}	R^2	$\varepsilon\%$	q_0	a	R^2	$\varepsilon\%$
0.4–0.8	85.02	0.02981	0.9826	46.1	2061	0.00164	0.9826	43.66	82.3	3.034	0.996	25.19
0.8–1.25	39.29	0.03479	0.879	107.28	1086	0.00191	0.8790	106.14	27.6	1.157	0.9627	59
1.25–2	10	0.1429	0.8416	158	297.5	0.00771	0.8448	147.55	12.8	1.021	0.9491	71.3
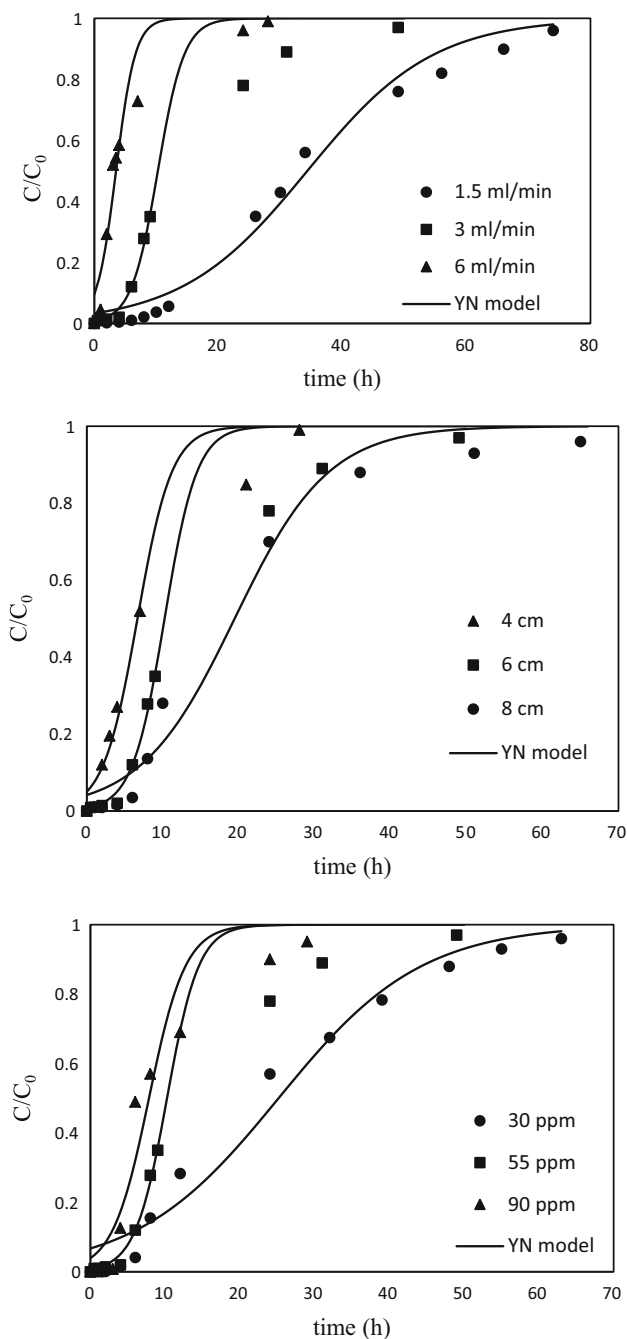
Fig. 7 Breakthrough curves for continuous thorium biosorption under different operating conditions with the Yoon–Nelson model at pH 3.8 and $T = 25$ °C

the electrostatic attraction between these functional groups and the metal cation. The carboxylic group loses proton at high pHs (–CO$\bar{\text{O}}$) and has a negative superficial potential, which increases the metal cation absorption capacity.

To determine the elements and their percentages in the adsorbent, XRF analysis was taken from the orange peel before and after saturation. The results of Table 4 show that the percentage of calcium and potassium ions decreased significantly after adsorption, and on the other hand, with the adsorption of thorium, the percentage of thorium in adsorbent after absorption increased (93% by weight). So calcium and potassium ions are replaced by thorium ions during the adsorption process. By measuring the concentrations of calcium and potassium ions in samples taken from the column outlet solution, can also study the mechanism of the process. In order to determine the concentrations of calcium and potassium ions in the column outlet solution, a set of experiments was carried out at a concentration of 90 mg/L with optimal absorbent particle size, as well as a height of 6 cm and a flow rate of 3 mL/ min. Changes in the concentration of calcium and potassium ions in the solution of the column output from time to time are shown in Fig. 10. According to this figure, it can be concluded that the calcium and potassium ions are replaced by thorium ions. At the beginning of the process because of the high adsorption rate, the amounts of calcium and potassium ions in the outlet solution are high and over time, since the rate of the adsorption is reduced, the amounts of calcium and potassium ions also decreased in the output solution. From Fig. 10, and the results of the XRF analysis (Table 4), it is evident that ion exchange is the dominant mechanism in the biosorption of thorium with orange peel.

The pH of the outlet solution from the column was also measured at concentrations of 30, 55 and 90 mg/L of inlet solution. According to Fig. 11, the pH of the outflow solution of the column has a sudden increase at the start of the absorption process, and then decreases over time, and finally approaches the pH of the inlet solution, i.e., 3.8. This can be attributed to the adsorption of thorium and the release of Ca^{2+} and K$^+$ ions from the orange peel to the solution. This observation confirms that ion exchange is
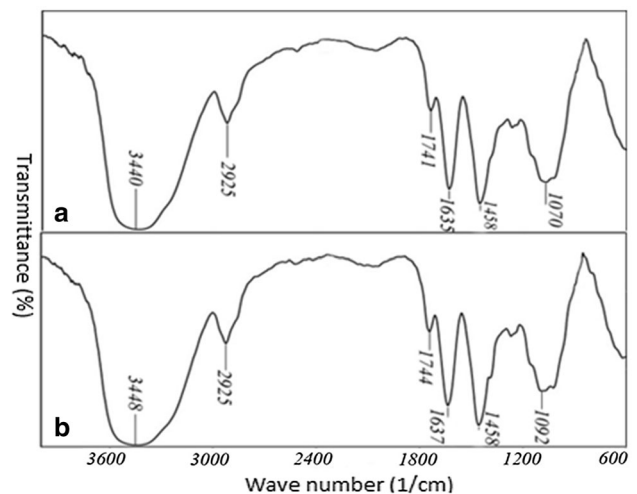
Fig. 9 FTIR spectrum of orange peel before adsorption of thorium (a), after absorption of thorium (b)

Table 4 XRF analysis of orange peel before and after the biosorption (saturated with thorium)

Analyte	Weight percent	
	Before biosorption	After biosorption
MgO	2.81	1
Al_2O_3	2.85	0.71
SiO_2	12.92	2
P_2O_5	2.22	0.25
SO_3	6.28	0
Cl	0.67	0
K_2O	19.85	0
CaO	44.5	1.34
Fe_2O_3	0.73	0.28
CuO	0.20	0.15
Zn	0.31	0.12
SrO	0.23	0
ThO_2	0	93

Fig. 8 Breakthrough curves for continuous thorium biosorption under various operating conditions with the MDR model at pH 3.8 and $T = 25$ °C

one of the main mechanisms for absorbing thorium with orange peel.

Conclusion

The breakthrough curves obtained from the biosorption of thorium are influenced by the size of the adsorbent particles, the bed height, the input concentration and the input flow rate. It was observed that with decreasing the bed height, increasing the size of the adsorbent particles and the inlet concentration and increasing the flow rate, the breakthrough point (time) decreases. Also, with the increase of the concentration and the flow rate, the amount of absorption capacity is high and low, respectively. The breakthrough curves obtained from the models were in good agreement with experimental results. According to the modeling, it can be said that the MDR model have a better agreement with experimental results.

According to the FTIR analysis of orange peel, there are abundant hydroxyl and carboxyl groups in this adsorbent that are involved in binding to thorium metal. The results
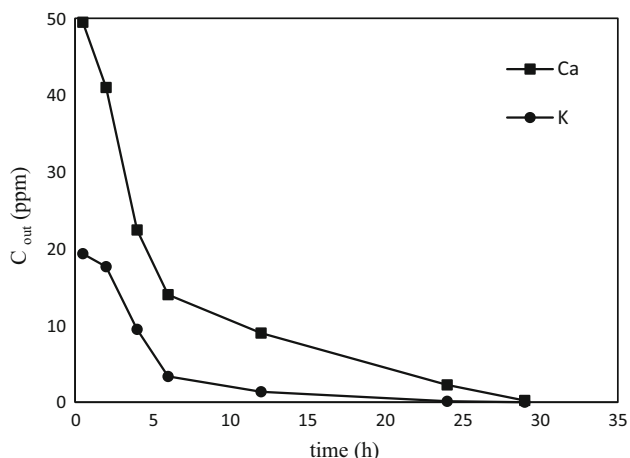
Fig. 10 Calcium and potassium ions in the outlet flow in time intervals, adsorbent particle size of 0.4–0.8 mm at pH 3.8 (height of the bed 6 cm, inlet concentration of 90 mg/mL and flow rate of 3 mL/min)
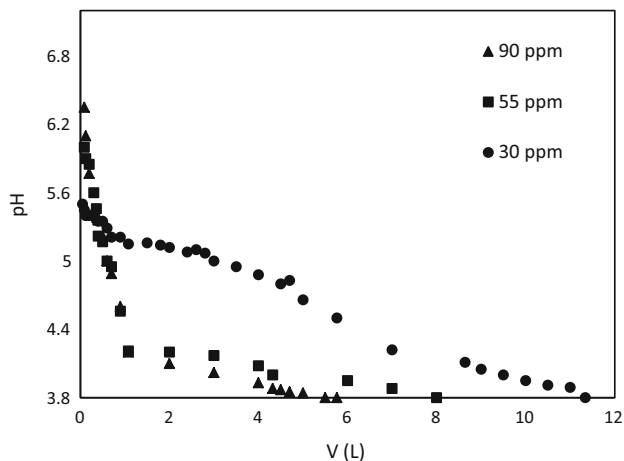
Fig. 11 pH variations of outlet flow of the column at flow rate of 3 mL/min and bed height of 6 cm

of XRF analysis and the concentration of calcium and potassium ions in the outlet solution showed that ion exchange is the dominant mechanism for absorbing thorium on the orange peel.

References

1. Furukawa K, Arakawa K (2008) A road map for the realization of global-scale thorium breeding fuel cycle by single molten-fluoride flow. Energy Convers Manag 49:1832–1848
2. Wickleder MS, Fourest B, Dorhout PK (2010) The chemistry of the actinide and transactinide elements. Springer, Berlin
3. Bhainsa KC, D'Souza SF (2009) Thorium biosorption by *Aspergillus fumigatus*, a filamentous fungal biomass. J Hazard Mater 165:670–676
4. Volesky B (2003) Sorption and biosorption. BV-Sorbex, Montreal
5. Walton HF, Rocklin RD (1990) Ion exchange in analytical chemistry. CRC Press, Boca Raton
6. Keim R (1993) Gmelin handbook of inorganic chemistry, uranium supplement, cation-exchange and chromatography. Springer, Berlin
7. Demirel N, Merdivan M (2003) Thorium(IV) and uranium(VI) sorption studies on octacarboxymethyl-C-methylcalix resorcinarene impregnated on a polymeric support. Anal Chim Acta 485:213–219
8. Talip Z, Eral M, Hicsonmez U (2009) Adsorption of thorium from aqueous solutions by perlite. J Environ Radioact 10:139–143
9. Metaxas M, Kasselouri-Rigopoulou V, Galiatsatou P, Konstantopoulou C, Oikonomou D (2003) Thorium removal by different adsorbents. J Hazard Mater 97:71–82
10. Dyer A, Jozefowicz LC (1992) The removal of thorium from aqueous solutions using zeolites. J Radioanal Nucl Chem 159:47–62
11. Pamukoglu MY, Kirkan B, Senyurt M (2017) Removal of thorium(IV) from aqueous solution by biosorption onto modified powdered waste sludge: experimental design approach. J Radioanal Nucl Chem 314:343–352
12. Gao Y, Hou D, He DX, Jiang M, Yang XC, Liao S, Zhang W, Yan XM, Tan N (2017) Higher uranium(VI) biosorption capacity and repeated use of PA-ZZF51 prepared by marine mangrove endophytic fungus ZZF51 and phytic acid. J Radioanal Nucl Chem 314:1915–1925
13. Huang G, Chen Z, Wang L, Lu TT, Shi J (2016) Removal of thorium(IV) from aqueous solution using magnetic ion-imprinted chitosan resin. J Radioanal Nucl Chem 310:1265–1272
14. Lu D, Cao Q, Li X, Cao X, Luo F, Shao W (2009) Kinetics and equilibrium of Cu(II) adsorption onto chemically modified orange peel cellulose biosorbents. Hydrometal 95:145–152
15. Schiewer S, Iqbal M (2010) The role of pectin in Cd binding by orange peel biosorbents: a comparison of peels, depectinated peels and pectin acid. J Hazard Mater 177:899–907
16. Chatterjee A, Schiewer S (2011) Biosorption of cadmium (II) ions by citrus peels in a packed bed column: effect of process parameters and comparison of different breakthrough curve models. CLEAN Soil Air Water 39:874–881
17. Perez Marin AB, Aguilar MI, Meseguer VF, Ortuno JF, Saez J, Llorens M (2009) Biosorption of chromium(III) by orange (*Citrus sinensis*) waste: batch and continuous studies. Chem Eng J 155:199–206
18. Movafaghpour A (2013) Kinetic and isotherm studies for biosorption of thorium on orange peel. M.Sc. thesis, Tehran University
19. Malkoc E, Nuhoglu Y (2006) Removal of Ni(II) ions from aqueous solutions using waste of tea factory: adsorption on a fixed-bed column. J Hazard Mater 135:328–336
20. Baral SS, Das N, Ramulu TS, Sahoo SK, Das SN, Chaudhury GR (2009) Removal of Cr(VI) by thermally activated weed *Salvinia cucullata* in a fixed-bed column. J Hazard Mater 161:1427–1435
21. Singh A, Kumar D, Gaur JP (2012) Continuous metal removal from solution and industrial effluents using Spirogyra biomass-packed column reactor. J Water Res 46:779–788
22. Lasheen MR, Ammar NS, Ibrahim HS (2012) Adsorption/desorption of Cd(II), Cu(II) and Pb(II) using chemically modified orange peel: equilibrium and kinetic studies. Solid State Sci 14:202–210
23. Gnanasambandam R, Proctor A (2000) Determination of pectin degree of esterification by diffuse reflectance Fourier transform infrared spectroscopy. Food Chem 68:327–332